

Enhanced secondary ion emission with a bismuth cluster ion source

G. Nagy, A.V. Walker*

Department of Chemistry, Washington University in St. Louis, Campus Box 1134, One Brookings Drive, St. Louis, MO 63130, United States

Received 24 August 2006; received in revised form 5 November 2006; accepted 6 November 2006

Available online 1 December 2006

Abstract

We have investigated the mechanism of secondary ion yield enhancement using Bi_n^+ ($n=1-6$) primary ions and three different samples – DL-phenylalanine, Irganox 1010 and polystyrene – adsorbed on Al, Si and Ag substrates. The largest changes in secondary ion yields are observed for Bi_2^+ and Bi_3^+ primary ions. Smaller increases in secondary ion yield are found using Bi_4^+ , Bi_5^+ and Bi_6^+ projectiles. The secondary ion yield enhancements are generally larger on Si than on Al. Using Bi_n^+ structures obtained from density functional theory (DFT) calculations we demonstrate that the yield enhancements cannot be explained by an increase in the deposited energy density (energy per area) into the substrate. These data show that the mechanism of Bi_n^+ sputtering is very similar to that for Au_n^+ primary ion beams. When a polyatomic primary ion strikes the substrate, its constituent atoms are likely to remain near to each other, and so a substrate atom can be struck simultaneously by multiple atoms. The action of these multiple concerted impacts leads to efficient energy transfer in the near surface region and an increase in the number of secondary ions ejected from the surface. Such concerted impacts involve one, two or three projectile atoms, which explains well the nonlinear yield enhancements observed going from Bi^+ to Bi_2^+ to Bi_3^+ .

© 2006 Elsevier B.V. All rights reserved.

Keywords: Secondary ion mass spectrometry; Nonlinear yield enhancement; Sputtering; Polyatomic ions

1. Introduction

Today secondary ion mass spectrometry (SIMS) is a widely used technique for the analysis of sample chemical composition in fields ranging from materials chemistry to biological systems [1,2]. One of the drawbacks of SIMS analysis is that low secondary ion yields are often observed for primary atomic ion impacts. Polyatomic projectiles have been demonstrated to greatly enhance molecular ion yields compared to monoatomic primary ion beams, such as Ga^+ or Ar^+ . Examples of polyatomic ion beams that exhibit this behavior include Au_n^+ [3–8], Au_n^- [9], SF_5^+ [10–13], C_{60}^+ [14–19], $(\text{CsI})_n\text{Cs}^+$ [20] and $(\text{Bi}_2\text{O}_3)_n\text{BiO}^+$ [20]. The use of polyatomic primary ions has led to improvements in the maximum spatial lateral resolution of SIMS mass spectrometric images (chemical images) [21]. Further, the accumulated sample (chemical) damage using polyatomic primary ion beams is greatly reduced compared to monoatomic ions. Hence, it has now become possible to perform molecular depth profiling [16].

The use of polyatomic projectiles in sputtering has been investigated since the 1960s [22–24]. At the energies used in our experiments (kinetic energy ≤ 100 keV) the predominant energy loss mechanism is nuclear stopping. In 1979, Johar and Thompson [25,26] observed that diatomic and triatomic P, As, Sb and Bi primary ions greatly increased the sputter yields from Ag, Au and Pt targets, and the yield was strongly nonlinear with the number of atoms in the projectile (a “nonlinear” yield enhancement). One important conclusion from this work was that the high sputtering yields were due to the polyatomic ions creating a “collisional” spike in the sample surface, rather than a “thermal spike” [27]. Studies by Benguerba et al. also supported the “collisional” spike mechanism [3]. These authors also concluded that the yield enhancements were dependent on the energy density (energy/area) deposited into the substrate surface by the projectile and not on the linear energy loss of the projectile (dE/dx where x is the penetration depth of the primary ion). This data supports the “collisional” spike mechanism since the energy density is dependent on the mass and size of the projectile; as the number of constituents in the projectile increases there is an overlap of collision cascades within the material leading to the enhanced sputter yield. Later studies using molecular and polymer substrates demonstrated that the enhanced sputter yield

* Corresponding author. Tel.: +1 314 935 8496; fax: +1 314 935 4481.
E-mail address: walker@wustl.edu (A.V. Walker).

was not accompanied by a proportional increase in the damage cross-section [10]. (The damage cross-section is determined by the average surface area damaged by a single ion impact. In this area, the surface is modified so that a secondary ion cannot be created from the surface at a later time.)

The mechanism of nonlinear yield enhancement has also been investigated by molecular dynamic (MD) simulations [15,28–32]. These simulations suggest that multiple collisions are needed to cause the ejection of a molecule into the gas phase. For a polyatomic projectile there is a higher probability that multiple collision cascades are generated simultaneously from the collision of the constituent projectile atoms with the substrate molecules/atoms. There is therefore an enhancement in the observed sputter yield due to the “nonadditive” effects of the collision cascades. Further these simulations have shown that the substrate significantly influences the yield enhancement, with larger enhancements observed for less dense substrates, such as Si [31,32].

There were many drawbacks to the early polyatomic ion sources. They were often difficult to maintain, had low ion currents and could not be focused to small spot sizes. The recent developments of Au_n^+ , Bi_n^{x+} and C_{60}^+ primary ion sources have resolved many of these issues. The Au_n^+ and Bi_n^{x+} ion sources are liquid metal ion guns (LMIGs) [33]. They have long lifetimes $>500 \mu\text{A h}$, have a very high brightness, and can be focused to a spot size of 100 nm. These ion sources emit a variety of ions, necessitating the use of a mass filter to select the desired primary ion. Bi_n^{x+} ion sources produce higher cluster currents than Au_n^+ ion sources because a eutectic alloy is not required to lower the source operating temperature. Recently these ion sources have been used to obtain molecular images from tissues, single cells, and a wide variety of other samples [21,33,34]. The C_{60}^+ ion source has also been used to obtain molecular depth profiles [16].

In this paper we have investigated the mechanism of Bi_n^+ ($n=1\text{--}6$) secondary ion yield enhancements. We survey three different organic samples which are used in a variety of important medical and technological applications. Samples were prepared by forming thin films of polystyrene ($M_w=1110$), Irganox 1010 ($(M-H)^- m/z=1175$) and DL-phenylalanine ($(M+H)^+ m/z=166$) adsorbed on silver, aluminum and silicon substrates. DL-Phenylalanine is an amino acid, while Irganox 1010 and polystyrene are a commonly used polymer additive and polymer, respectively. Also, these samples have all often been characterized using TOF SIMS and were used in previous studies of secondary yield enhancements using Au_n^+ primary ions [3,4,7,35]. Fig. 1 displays their structures.

Using our results and data for Au_n^+ projectiles [4], we deduce a general mechanism for nonlinear yield enhancements for kilo-electronvolt polyatomic projectiles. Our studies suggest that the mechanism of nonlinear secondary ion yield enhancement involves multiple, concerted particle (Bi or Au) impacts on substrate atoms which leads to efficient energy transfer between the projectile and the substrate atoms in the near-surface region. Further this model explains the large changes in nonlinear yield enhancement observed going from Bi^+ to Bi_2^+ to Bi_3^+ , or Au^+ to Au_2^+ to Au_3^+ .

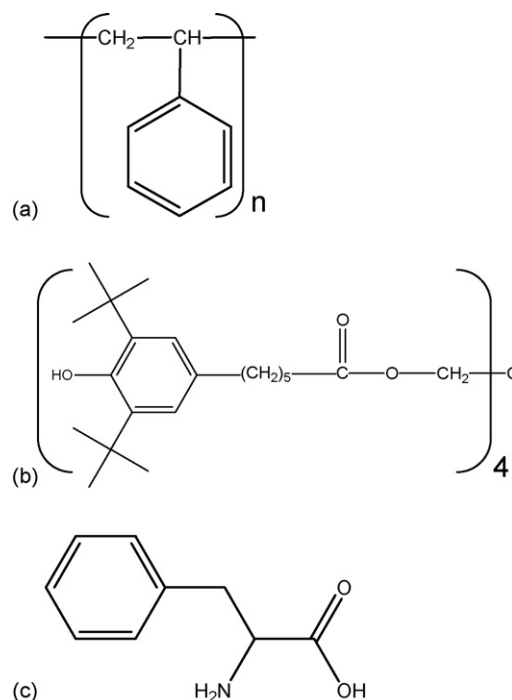


Fig. 1. The structure of (a) polystyrene, (b) Irganox 1010 and (c) DL-phenylalanine.

2. Experimental

2.1. Time-of-flight secondary ion mass spectrometry

Time-of-flight secondary ion mass spectra were obtained using a TOF SIMS IV instrument (ION TOF Inc., Chestnut Ridge, NY). The instrument consists of a loadlock, a preparation chamber and an analysis chamber, each separated by a gate valve. The preparation and analysis chambers were kept between 1×10^{-9} mbar and 5×10^{-9} mbar during experiments. The primary ion beam was generated using a liquid ion gun fitted with a pure Bi source, capable of producing Bi_n^+ ($n=1\text{--}6$) ions. The primary ions were mass selected using their flight time via a double blanking plate system, and their kinetic energy was varied from 10 keV to 25 keV. The primary ion beam current was measured prior to and after obtaining a TOF SIMS spectrum using a Faraday cup which is located on a grounded sample holder. The difference between the measured ion currents was at maximum $\pm 5\%$. Typical primary ion currents for a 25 keV beam energy are 1.0 pA (Bi^+), 0.46 pA (Bi_2^+), 0.35 pA (Bi_3^+), 0.13 pA (Bi_4^+) and 0.044 pA (Bi_5^+).

The secondary ions generated were extracted into a time-of-flight mass spectrometer using an energy of 2000 V. Before reaching the detector the secondary ions were reaccelerated to 10 keV.

Analyzed sample areas were $152 \mu\text{m} \times 152 \mu\text{m}$ for polystyrene adsorbed on silver foil, and Irganox 1010 and DL-phenylalanine adsorbed on silicon and aluminum. The primary ion dose during data acquisition was less than 10^{10} ions cm^{-2} which is below the static SIMS limit. The secondary ion peak intensities were reproducible $\pm 5\%$ from scan-to-scan.

and $\pm 15\%$ from sample-to-sample. The secondary ion yields reported are the average values calculated from three different samples with at least three spots per sample analyzed (i.e., nine measurements). The average calculated error in the secondary ion yields is $\pm 12\%$.

2.2. Sample preparation

Irganox 1010 was obtained from Ciba Specialty Chemicals (Tarrytown, NY), DL-phenylalanine from Sigma–Aldrich (St. Louis, MO) and narrow distribution polystyrene 771 ($M_w = 1110$) from Scientific Polymer Products, Inc. (Ontario, NY).

Irganox 1010 and polystyrene were dissolved in chloroform as 1.00 mg/ml solutions. A 10^{-2} M solution of DL-phenylalanine was prepared using a 1:1 2-propanol:water mixture as the solvent. Chloroform (EMD Chemical, Gibbstown, NJ) and 2-propanol (Fisher Scientific, Pittsburgh, PA) were high purity and HPLC grade, respectively.

The substrates used were silver foil (99.9% purity, 0.05 mm thick, Alfa Aesar, Ward Hill, MA), aluminum foil (99.99% purity, 0.1 mm thick, Alfa Aesar) and single crystal silicon wafer ($\langle 111 \rangle$ orientation, Addison Engineering, San Jose, CA). The Ag and Al foils were prepared by etching in 1:1 $\text{HNO}_3\text{:H}_2\text{O}$, rinsing several times in water, followed by rinsing in 2-propanol and drying with N_2 gas. The Si wafers were prepared using Piranha etch (1:3 $\text{H}_2\text{O}_2\text{:H}_2\text{SO}_4$), followed by rinsing with copious amounts of water and 2-propanol, and drying with N_2 gas.

Thin film samples of polystyrene and Irganox 1010 were prepared by spin coating in the following way: ~ 1.2 ml (polystyrene), or 0.6 ml (Irganox 1010), of solution was dropped onto a 1 cm^2 ($1\text{ cm} \times 1\text{ cm}$) substrate (silver foil, aluminum foil or silicon wafer) and the sample spun at 500 rpm for 12 s and then 2900 rpm for 10 s using a KW-4A spin-coater (Chemat Technology, Inc., Northridge, CA). Samples of DL-phenylalanine was prepared by allowing one drop of solution (< 0.1 ml) to evaporate on the substrate surface. We estimate that the sample films are 100–300 Å thick. In all SIMS spectra, we clearly observe ions from the substrate indicating that Bi_n^+ ions penetrate through the organic layer to the substrate.

2.3. Quantum mechanical calculations

To determine the cross-sectional area of the primary ion used, density functional theory (DFT) geometry optimization calculations were performed to determine the lowest energy structures with the formula Bi_n^+ and Bi_n ($n = 1\text{--}6$). The calculations were carried out at the PW91PW91/CRENBL level of theory [36–42] using the NWChem 4.5 package [43]. The accuracy of the computational method was checked by benchmark calculations on the Bi atom and Bi_2 cluster. From our calculations the ionization potential and electron affinity of Bi are 8.03 eV and 0.69 eV, in good agreement with experimental data, 7.29 eV and 0.95 eV, respectively [44]. For Bi_2 , the ionization potential is 7.44 eV, which is also in good agreement with experimental data [45]. However the binding energies of Bi_2 and Bi_2^+ are much larger, 5.1 eV and 5.7 eV respectively, than the experimentally observed

values, 2.06 eV [46] and 1.77 eV [47], respectively. At present it is not clear why the calculated binding energies of Bi_2 and Bi_2^+ differ from the experimental values. We note that we also calculated these structures at the PW91PW91/LANL2DZdp level of theory [36,48–50], and nearly-identical lowest-energy structures were found. These structures are also in agreement with previous studies of Bi cluster structures [51]. Further, the structures calculated follow Wade's rules for cluster structures [52,53]. Thus we believe that the reported structures are the lowest-energy Bi cationic structures. We are currently working on improving the calculational methods employed to reproduce the ionization potentials, electron affinities and bond energies more accurately.

2.4. Calculation of the average cross-sectional area of the Bi_n^+ clusters

The geometry-optimized lowest-energy Bi_n^+ clusters were used to calculate the minimum, maximum and orientationally-averaged cross-sectional areas of the primary ions used in these studies.

The calculation was carried out in the following way. Using Cartesian coordinates of the Bi atoms in the cluster and an atomic radius of 1.60 Å for Bi [54], a space filling model of the Bi_n^+ cluster was evaluated by projection onto a planar surface. To obtain the orientationally-averaged cross-sectional area, this area was recalculated for each possible Eulerian orientation of the cluster, $\phi = 0\text{--}360^\circ$, $\theta = 0\text{--}180^\circ$ and $\psi = 0\text{--}360^\circ$, and the average of these areas determined.

3. Results

3.1. Effect of Bi_n^+ ($n = 1\text{--}6$) projectile velocities on secondary ion yields

The secondary ion yields, Y , of Irganox 1010, polystyrene and DL-phenylalanine were calculated from their mass spectra. Fig. 2 displays an example of the data obtained: the secondary ion yields of Irganox 1010 molecular ion $((M - \text{H})^-; m/z = 1175)$ and several fragment ions ($\text{C}_{17}\text{H}_{25}\text{O}_3^-$, (monomer) $^-$, $m/z = 277$; $\text{C}_{56}\text{H}_{83}\text{O}_{10}^-$, ((monomer) $_3\text{--C--CH}_2\text{O})^-$, $m/z = 915$) from a thin film adsorbed on a Si substrate bombarded with Bi_n^+ ($n = 1\text{--}6$) primary ions. Similar behavior is observed for DL-phenylalanine and polystyrene (data not shown). The secondary ion yields are presented as a function of the kinetic energy per constituent atom of the primary ion (which is proportional to v^2 , where v is the primary ion velocity) so that the secondary ion yields obtained with different Bi cluster projectiles can be compared at the same impact velocity. For a given Bi_n^+ primary ion we observe that the secondary ion yield increases linearly with the incident kinetic energy per Bi atom (i.e., with v^2) (Fig. 2).

Similar behavior has been observed for Au_n^+ clusters incident on organic surfaces [3,4], indicating that the mechanism of Bi_n^+ secondary ion yield enhancement is similar to that for Au_n^+ . A further indication that the mechanism of Bi_n^+ is similar to that Au_n^+ sputtering is that the largest increases in secondary ion yield occurs when changing from Bi^+ to Bi_2^+ and Bi_3^+ primary ion bombardment (Fig. 2).

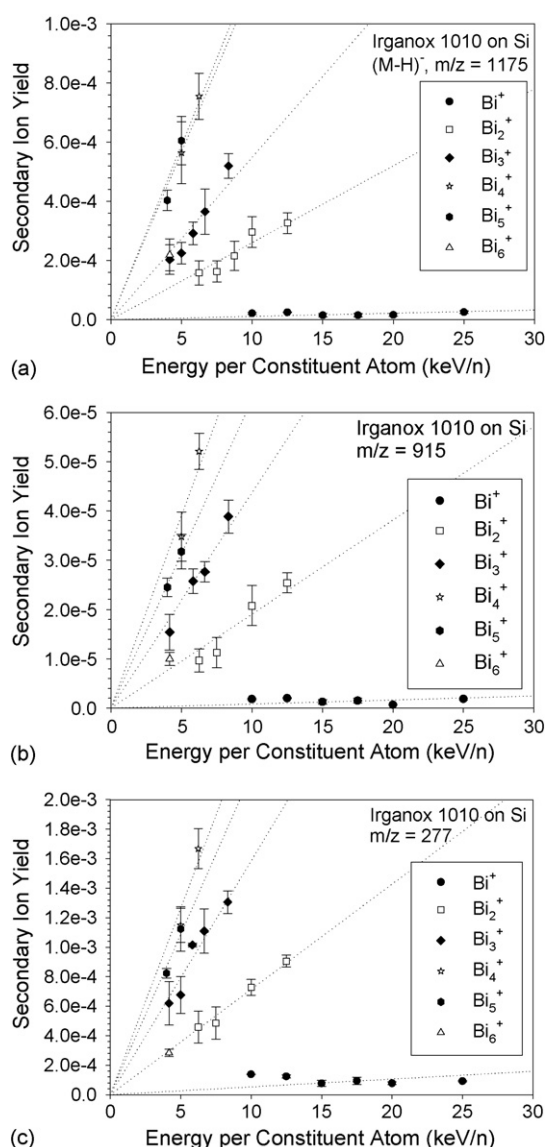


Fig. 2. The secondary ion yields of Irganox 1010 spin coated on a Si substrate from negative ion mode spectra: (a) $m/z = 1175$, (b) $m/z = 915$ and (c) $m/z = 277$. Secondary ion yields from Bi^+ primary ions are shown as filled circles, Bi_2^+ open squares, Bi_3^+ filled diamonds, Bi_4^+ open stars, Bi_5^+ filled hexagons and Bi_6^+ open triangles. The dotted lines are drawn as a guide to the eye.

Secondary ion yields for bombardment of Irganox 1010, DL-phenylalanine and polystyrene films with Bi_n^+ ($n=1-4$) for Bi_2^+ , Bi_3^+ and Bi_4^+ , with respect to Bi^+ at constant primary ion energy, 25 keV, are given in

Table 1. For Irganox 1010 ($M-H)^-$ ($m/z=1175$), the ratios of the secondary ion yields are 1:13.0:24.6:35.6:28.5:8.7 for $\text{Bi}^+:\text{Bi}_2^+:\text{Bi}_3^+:\text{Bi}_4^+:\text{Bi}_5^+:\text{Bi}_6^+$ primary ion bombardment. For DL-phenylalanine ($M+H)^+$ ($m/z=166$) the secondary ion yield ratios are 1:7.0:9.4:20.9:13.2:7.1, and for polystyrene adsorbed on silicon ($m/z=1008$ positive ion mode) 1:43.8:71.4:92.4:84.6:61.6. We note that the secondary ion yields using Bi_6^+ primary ion beams are most likely underestimated, and we estimate the error may be as large as 25%. (This is due to uncertainties in measuring the primary ion beam current. The current may be lower than reported since we are near to the limit of detection for the Bi_6^+ primary ion current (typical Bi_6^+ ion current ~ 0.01 pA and the lowest ion current that can be detected is 0.004 pA).) A useful parameter to discuss these ion yields is the yield enhancement, YE, which is defined as $YE = Y_n(E)/nY_1(E/n)$ where $Y_n(E)$ is the secondary ion yield measured for Bi_n^+ primary ion bombardment, n is the number of constituent atoms in the polyatomic primary ion and $Y_1(E/n)$ is the secondary ion yield observed for Bi^+ projectiles measured at the same velocity. If $YE > 1$, the yield enhancement is said to be nonlinear, i.e., more secondary ions are produced than would be expected if the secondary ion yield was proportional to the primary ion size, where $Y_n(E) = nY_1(E/n)$. The yield enhancements for Bi_2^+ , Bi_3^+ and Bi_4^+ primary ion bombardment are shown in Table 1. We observe nonlinear yield enhancements for all systems studied except for polystyrene adsorbed on Ag. We note that Ag substrates are well known cationizing agents and greatly increases the observed ion yield from polystyrene [2]. For Bi^+ primary ions, the secondary ion yield for polystyrene adsorbed on Ag is approximately 100 times larger than when it is adsorbed on Si (Table 1). Finally, we note that the yield enhancements observed are lower than those observed using Au_n^+ primary ion bombardment [3,4].

The number of secondary ion generated from a molecular layer is dependent not only on its ionization probability and the primary ion current but also on the sputter rate of the material [55]. One important parameter to determine is the whether the secondary ion yield increases relative to the amount of material removed from the surface. To measure this, the efficiency, e , which is the ion yield relative to the disappearance cross-section, has been determined. The disappearance (damage) cross-sections, σ , is measured by following the decrease of mass spectra peaks with ion dose. We note that the decrease in the ion intensity is due to either (or both) the sputtering (removal) of the analyte from the surface or the destruction of

Table 1

Molecular ion yields and yield enhancements for thin films of Irganox 1010, DL-phenylalanine upon Bi^+ , Bi_2^+ , Bi_3^+ , Bi_4^+ primary ion bombardment at a kinetic energy of 25 keV

Sample	Molecular ion; mass (Da)	Y_{Bi^+}	$Y_{\text{Bi}_2^+}$	$Y_{\text{Bi}_3^+}$	$Y_{\text{Bi}_4^+}$	$YE^a (\text{Bi}_2^+)$	$YE^a (\text{Bi}_3^+)$	$YE^a (\text{Bi}_4^+)$
Irganox 1010 on Si	$(M-H)^-$; 1175	2.1×10^{-5}	3.3×10^{-4}	5.2×10^{-4}	7.6×10^{-4}	6.5	8.2	8.9
DL-Phenylalanine on Al	$(M+H)^+$; 166	9.4×10^{-4}	3.3×10^{-3}	3.2×10^{-3}	7.1×10^{-3}	3.5	3.1	5.2
Polystyrene on Ag	$(M_{12} + \text{Ag})^+$; 1413	7.1×10^{-5}	1.4×10^{-4}	1.3×10^{-4}	2.7×10^{-4}	1.0	0.60	0.9
Polystyrene on Si	$\text{C}_{72}\text{H}_{144}^+$; 1008	1.3×10^{-7}	5.7×10^{-6}	9.3×10^{-6}	1.2×10^{-5}	21.9	23.8	23.1

^a The yield enhancements for Bi_3^+ and Bi_4^+ are calculated using the secondary ion yields for a Bi^+ of 10 keV. This is lowest energy at which the Bi_n^+ primary ion beam is stable.

Table 2

Secondary ion yields, Y , disappearance cross-section, σ , and ion bombardment efficiencies, e , for Bi_n^+ bombardment on Irganox 1010 ($(M-H)^- m/z=1175$) adsorbed on silicon and polystyrene ($(M_{12}+Ag)^+ m/z=1413$) adsorbed on silver

Projectile	Y	$\sigma \text{ (cm}^2\text{)}$	$e \text{ (cm}^{-2}\text{)}$
Irganox 1010 on Si			
Bi^+	2.1×10^{-5}	6.9×10^{-14}	3.0×10^8
Bi_2^+	3.3×10^{-4}	1.3×10^{-13}	2.5×10^9
Bi_3^+	5.2×10^{-4}	1.4×10^{-13}	3.7×10^9
Bi_4^+	7.6×10^{-4}	1.8×10^{-13}	4.2×10^9
Bi_5^+	6.1×10^{-4}	1.2×10^{-13}	5.1×10^9
Polystyrene on Ag			
Bi^+	7.1×10^{-5}	1.1×10^{-13}	6.7×10^8
Bi_2^+	1.4×10^{-4}	1.4×10^{-13}	1.0×10^9
Bi_3^+	1.3×10^{-4}	1.9×10^{-13}	6.8×10^8
Bi_4^+	2.7×10^{-4}	2.6×10^{-13}	1.1×10^9
Bi_5^+	2.1×10^{-4}	2.7×10^{-13}	7.6×10^8

Primary ion energy 25 keV.

the analyte chemical structure by ion bombardment. Table 2 displays the secondary ion yield, disappearance cross-section and efficiencies for Irganox 1010 adsorbed on Si and polystyrene adsorbed on Ag under Bi_n^+ bombardment. Fig. 3 displays the logarithm of the intensity of Irganox 1010 molecular ions generated ($(M-H)^- m/z=1175$) as a function of ion dose. It can be seen that the ion signals decrease exponentially with ion dose. Similar behavior is observed for all the analytes and their fragment ions (data not shown). The resulting disappearance cross-sections for Bi cluster ion bombardment are within a factor of three of the Bi^+ primary ions. Thus the increases observed in the secondary ion yields are not due to enhanced chemical damage of the sample. We note that for polystyrene adsorbed on Ag, which does not exhibit nonlinear secondary ion yield enhancement, the efficiency of the ion generation for Bi cluster ion bombardment was similar to, or slightly better than for Bi^+ ion bombardment (Table 2). This further supports the hypothesis that the increase in ion yield is not due to an increase in the chemical damage.

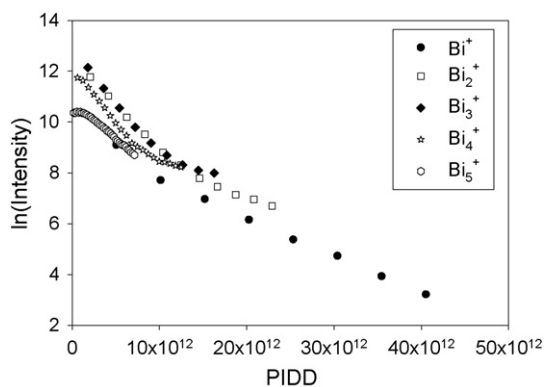


Fig. 3. Logarithm of the intensity of the molecular intensity $(M-H)^-$ ($m/z=1175$) plotted vs. primary ion dose (PID) from an Irganox 1010 film adsorbed on Si.

3.2. Fragment ion formation

Although it is now agreed that polyatomic projectiles significantly enhance molecular secondary ion yields, it is not clear that the yield of fragment ions is increased. Using Au_n^+ ($n=1-5$) primary ions, Benguerba et al. observed that for a DL-phenylalanine film the yield of light such as H^- increased linearly with the number of atoms in the projectile [3]. However, Davies et al. observed that for a gramicidin A ($m/z \sim 1880$) film adsorbed on Al the yield enhancement for ions below $m/z=100$ was approximately same order as magnitude as for the quasi-molecular ion ($m/z=193$) [8]. Above $m/z=200$, the yield enhancement was found to significantly increase. Using C_{60}^+ primary ions and a

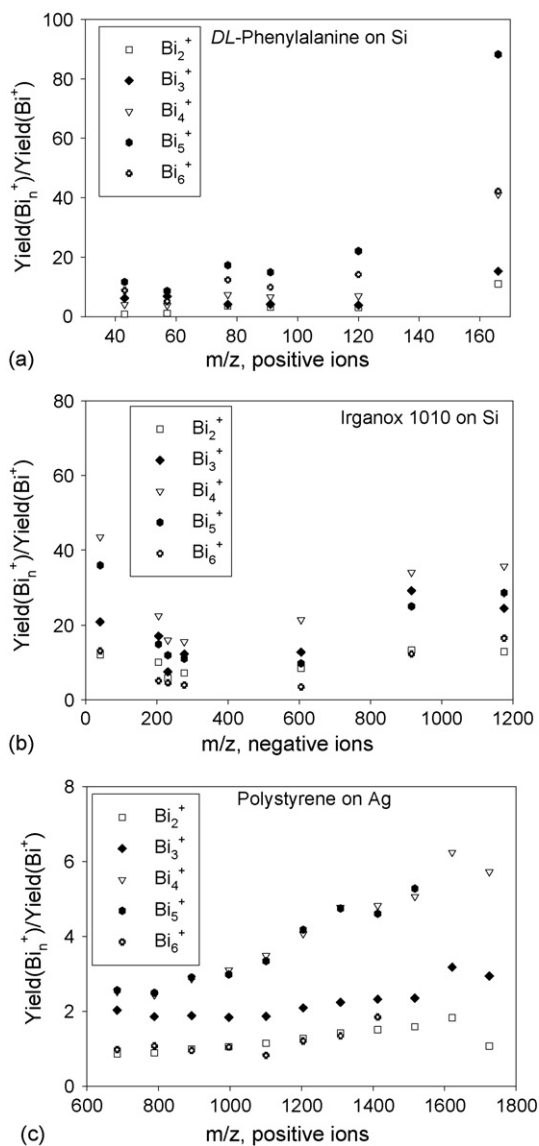


Fig. 4. Yield ratios ($Y(\text{Bi}_n^+)/Y(\text{Bi}^+)$) at constant primary ion velocity vs. m/z for thin films of (a) DL-phenylalanine on a Si substrate, (b) Irganox 1010 on a Si substrate and (c) polystyrene on a Ag substrate. The total energy of the Bi_n^+ ($n=2,3,4,5,6$) primary ion was 25 keV. The ratios for Bi_3^+ , Bi_4^+ , Bi_5^+ and Bi_6^+ were determined using a Bi^+ primary ion energy of 10 keV. This was the lowest energy that the Bi^+ ion beam was stable. Error bars have been removed from the figures to make them clearer. Typical error is $\pm 20\%$.

wide variety of films including polystyrene (PS-2000), Gramicidin D and Irganox 1010, the same research group showed that the fragment ion yield enhancements observed were dependent on the chemical identity of the analyte [19]. In later experiments Nagy and Walker [4] using Au_n^+ ($n = 1, 2, 3, 5, 7$) primary ions demonstrated that the secondary ion yield enhancements for fragment ions depend not only on the chemical identity of the analyte but on the mass of the ion as well. For example, in the case of Irganox 1010 adsorbed on Si, the yield enhancement initially decreases to a minimum at $m/z = \sim 500$ and then increases to the mass of the molecular ion $((M - H)^-; m/z = 1175)$. In contrast, for DL-phenylalanine the yield enhancements of fragment ions increased with increasing mass-to-charge ratio (m/z), and in for polystyrene adsorbed on Ag, the yield enhancement remained approximately constant in the n -mer region ($m/z = 600\text{--}1700$).

In our experiments using Bi_n^+ primary ions, we observe similar results to those observed for Au_n^+ primary ion bombardment (Fig. 4 and Tables 3 and 4) and provide another indication that Bi_n^+ sputtering mechanism is similar to that for Au_n^+ . In the case of DL-phenylalanine the ratio of the secondary ion yields increases from a mass-to-charge ratio of 43–166 $((M + H)^+)$ (Fig. 4a and Table 3). For Irganox 1010, the ratio of secondary ion yield decreases to minimum at $m/z = \sim 500$ and then increases to the mass of the molecular ion $(M - H)^-, m/z = 1175$ (Fig. 4b and Table 4). In the n -mer region of polystyrene adsorbed on Si, Al or Ag, we observe that the ratio of the secondary ion yields is approximately constant (Fig. 4c).

Following the interpretation of Walker and co-workers [4], as the number of Bi atoms in the primary ion increases the energy deposited in the surface region increases leading to an increase

Table 3

A comparison of the secondary ion yield and ratios of ion yields using Bi^+ and Bi_4^+ primary ion bombardment at the same ion velocity on thin films of DL-phenylalanine adsorbed on Si and Al substrates

Substrate	m/z	Y_{Bi^+} (10 keV) ^a	$Y_{\text{Bi}_4^+}$ (25 keV) ^a	$E_{\text{Si}} = Y_{\text{Bi}_4^+}/Y_{\text{Bi}^+}$ ^b	$E_{\text{Al}} = Y_{\text{Bi}_4^+}/Y_{\text{Bi}^+}$ ^b	$E_{\text{Si}}/E_{\text{Al}}$
Negative ions						
Si	164	1.5×10^{-4}	2.7×10^{-3}	18.7		1.04
Al	164	9.0×10^{-5}	1.6×10^{-3}		17.9	
Positive ions						
Si	43	5.1×10^{-4}	2.1×10^{-3}	4.12		1.56
Al	43	4.8×10^{-4}	1.3×10^{-3}		2.64	
Si	57	5.4×10^{-4}	2.1×10^{-3}	3.78		1.85
Al	57	3.8×10^{-4}	7.8×10^{-4}		2.04	
Si	91	9.5×10^{-4}	6.3×10^{-3}	6.65		0.96
Al	91	7.9×10^{-4}	5.5×10^{-3}		6.91	
Si	120	1.5×10^{-3}	1.0×10^{-2}	6.91		1.03
Al	120	1.2×10^{-3}	7.9×10^{-3}		6.68	
Si	166	3.0×10^{-4}	1.2×10^{-2}	41.06		1.98
Al	166	3.4×10^{-4}	7.1×10^{-3}		20.70	

^a The ratios are calculated using the secondary ion yields for a Bi^+ of 10 keV, and not 6.25 keV. This is because the Bi_n^+ primary ion beam is not stable below a kinetic energy of 10 keV.

^b The error in the yield ratio, E , is $\pm 20\%$. The error is calculated from the error in the secondary ion yields, which are not shown for clarity.

Table 4

A comparison of the secondary ion yield and ratios of ion yields using Bi^+ and Bi_4^+ primary ion bombardment at the same ion velocity on thin films of Irganox 1010 adsorbed on Si and Al substrates

Substrate	m/z	Y_{Bi^+} (10 keV) ^a	$Y_{\text{Bi}_4^+}$ (25 keV) ^a	$E_{\text{Si}} = Y_{\text{Bi}_4^+}/Y_{\text{Bi}^+}$ ^b	$E_{\text{Al}} = Y_{\text{Bi}_4^+}/Y_{\text{Bi}^+}$ ^b	$E_{\text{Si}}/E_{\text{Al}}$
Negative ions						
Si	41	1.9×10^{-4}	8.4×10^{-3}	3.49		1.20
Al	41	8.3×10^{-5}	3.0×10^{-3}		36.28	
Si	205	2.5×10^{-5}	5.7×10^{-4}	22.51		1.66
Al	205	6.1×10^{-5}	8.3×10^{-4}		13.54	
Si	231	3.2×10^{-4}	5.1×10^{-3}	15.97		1.19
Al	231	1.5×10^{-4}	2.0×10^{-3}		13.44	
Si	277	1.1×10^{-4}	1.7×10^{-3}	15.45		1.42
Al	277	7.3×10^{-5}	7.9×10^{-4}		10.88	
Si	607	1.2×10^{-6}	2.6×10^{-5}	21.46		1.11
Al	607	1.6×10^{-6}	3.0×10^{-5}		19.42	
Si	915	1.5×10^{-6}	4.9×10^{-5}	33.93		1.60
Al	915	1.0×10^{-6}	2.2×10^{-5}		21.17	
Si	1175	2.1×10^{-5}	7.6×10^{-4}	35.61		1.08
Al	1175	1.1×10^{-5}	3.6×10^{-4}		33.12	

^a The ratios are calculated using the secondary ion yields for a Bi^+ of 10 keV, and not 6.25 keV. This is because the Bi_n^+ primary ion beam is not stable below a kinetic energy of 10 keV.

^b The error in the yield ratio, E , is $\pm 20\%$. The error is calculated from the error in the secondary ion yields, which are not shown for clarity.

in surface damage (which is approximately proportional to the increase in cluster ion area and therefore the number of constituent atoms in the cluster). Hence, close to the primary ion impact point there is an increase in analyte fragmentation, and an approximately linear increase in the yield of very light fragment ions. Molecules slightly further away from the primary ion impact point desorb intact but are sufficiently excited to fragment before reaching the detector. For the Irganox 1010 samples, the yield enhancement decreases to a minimum at $m/z \sim 500$. Fragment ions of $m/z < 500$ derive from the Irganox 1010 monomer. As the number of ions in the projectile increases, there is an increase in the energy transferred to the analyte, which leads to a larger number of ejected fragments and monomers (neutrals or ions) ($m/z = 200$ –500) with sufficient energy to fragment into lighter mass ions ($m/z < 200$) before reaching the detector. Thus a higher number of lower mass ions ($m/z < 200$) are detected leading to the observed larger yield enhancements than for ions with m/z between 200 and 500. Heavier fragments and molecular ions ($m/z > 500$) are formed by the “lift off” mechanism in which whole molecules/large fragments are gently ejected by the concerted upward motion of substrate atoms. As the number of Bi atoms in the cluster increases more energy is deposited in the near surface region and this process becomes more likely. For Irganox 1010, the secondary ion yield enhancements increase above $m/z > 500$, with the largest enhancement observed for the molecular ion $(M - H)^-$ ($m/z = 1175$). For polystyrene adsorbed on Si, Al and Ag, the secondary ion yield enhancements remain approximately constant between $m/z = 500$ and 1800. In this case the secondary ions ejected contain integer numbers of the monomer.

3.3. Substrate structure

Secondary ion yield enhancements are dependent on the substrate structure and composition as well as the chemical identity of the analyte. Using MD simulations Krantzman and co-workers observed larger yield enhancements for less dense substrates, such as Si [31,32]. This observation was later experimentally confirmed by Walker and co-workers [4]. Using Au_n^+ primary ions they observed for Irganox 1010 and DL-phenylalanine adsorbed on Si (atomic weight: 28.086; diamond structure; density 2.33 g cm^{-3} [44]) and Al (atomic weight: 26.982; face-centered cubic structure; density 2.70 g cm^{-3} [44]) surfaces that the observed secondary ion yield enhancement was slightly larger (typically 1.1–2.0 times larger) for films adsorbed on the more open Si substrate. We note that for Au_3^+ ions bombarding DL-phenylalanine, the secondary ion yield enhancement was much larger: for the positive molecular ion $(M + H)^+$ ($m/z = 166$), the yield enhancement was 18 times larger on the Si substrate than on the Al substrate.

We have also examined the effect of substrate on secondary ion yields using thin films of DL-phenylalanine, Irganox 1010 and polystyrene adsorbed on Si and Al substrates. For DL-phenylalanine, in the positive ion mode we observe that the yield enhancement is larger on a Si substrate than on Al substrates (1–2 times), while in the negative ion mode the yield enhancement is slightly lower on the Si substrate (Table 3). We

note that for the $(M - H)^-$ ion, the secondary ion yield on a Si substrate is almost twice the observed ion yield on an Al substrate for Bi^+ ion bombardment, whereas the ion yields for Bi_n^+ bombardment are approximately the same on Si and Al. Thus, the yield enhancement is smaller on silicon than on aluminum. In the case of Irganox 1010, we observe that the yield enhancement is 1–2 times larger on Si than on Al (Table 4) in agreement with previous measurements using Au_n^+ primary ions [4]. For polystyrene, we observe that the on the more open Si substrate the yield enhancement is 3–5 times larger than on the Al substrate (data not shown). Taken together, these data suggest that there is a slight increase in the secondary ion yield enhancement on the more open silicon surface than on the more dense aluminum surface. We further note that we only observe the differences in the yield enhancement for certain ions. For example, for DL-phenylalanine the yield enhancements observed are within experimental error for the $(M - H)^-$ ion, but the yield enhancement is ~ 2 times larger for the $(M + H)^+$ ion.

4. Discussion

These studies indicate that the mechanism of Bi_n^+ ($n = 1$ –6) sputtering is very similar to that observed for Au_n^+ primary ions. Both Bi [[21,33] and this work] and Au [3–8] polyatomic projectiles greatly enhance molecular secondary ion yields with nonlinear yield enhancements as large as 30. The secondary ion yields of fragments ions are also enhanced. Furthermore the increase in secondary ion yields is not due to an increase in surface chemical damage: the secondary ion yields increases far faster than the measured damage cross-sections.

We note that we do observe some differences between Bi_n^+ and Au_n^+ sputtering. In general, the secondary ion yield enhancements for Bi_n^+ are slightly lower than those observed for Au_n^+ [4]. Indeed for polystyrene adsorbed on Ag we observe that the secondary ion yield enhancements observed are linear, not nonlinear. Secondary ion yields are dependent on both the sputter rate and the ionization probability [2]. Fig. 5 displays the variation of secondary ion yields of Irganox 1010 $(M - H)^-$ ($m/z = 1175$) with kinetic energy per atom upon bombardment by Bi_n^+ ($n = 1$ –6) and Au_n^+ ($n = 1$ –7) [4]. The secondary ion

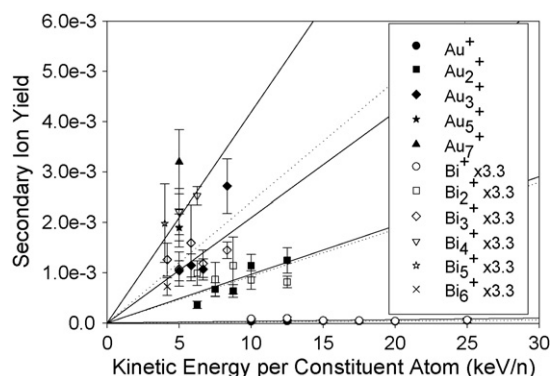


Fig. 5. The secondary ion yields of the molecular ion $(M - H)^-$ ($m/z = 1175$) from a thin film of Irganox 1010 spin coated on a Si substrate. Secondary ion yields from Au_n^+ primary ions are shown as filled shapes, and Bi_n^+ as open shapes. The dotted lines are drawn as a guide to the eye.

yields for Bi_n^+ primary ions have been multiplied by 3.3. It can clearly be seen in Fig. 5 that within the errors of the measurements ($\pm 15\%$) that the variation of the secondary ion yields with kinetic energy per atom are very similar for Bi_n^+ and Au_n^+ projectiles. Since the masses of Au ($A_r = 196.97$) and Bi ($A_r = 208.98$) are very similar, it is likely that the sputter rate will be approximately the same for these cluster projectiles. Thus the differences secondary ion yields are due to differences in the ionization probability.


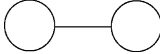
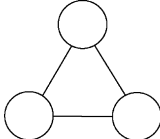
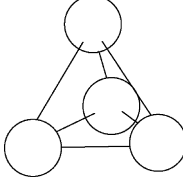
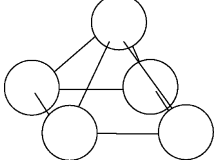
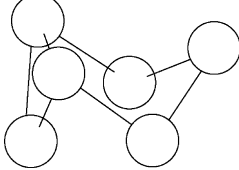
At first glance this suggests that Au_n^+ primary ions are better for SIMS analyses. However, Bi_n^+ primary ions have several advantages. Bismuth LMIG sources emit larger clusters and produce higher cluster ion currents [33]. For example, Bi_3^+ primary ion currents are about 25% of the emitted beam while Au_3^+ ions constitute only 5% of the primary ion beam. Thus, data can be acquired much faster when using a Bi_n^+ primary ion beam, which makes it possible to image biological samples, for example, in a reasonable time with useful lateral resolutions of less than 500 nm [21]. Secondly, bismuth LMIGs emit doubly charged ions, Bi_n^{2+} ($n = 1, 3, 5$), which have can be used to image surfaces with higher very high lateral resolution (< 400 nm) and also greatly increase secondary ion yields [21,56].

4.1. Mechanism of nonlinear secondary ion yield enhancement

The mechanism of nonlinear yield enhancement is not fully understood. It is correlated with kinetic energy per constituent atom of the primary ion (keV/n), but not the primary ion kinetic energy. It has been suggested that the nonlinear yield enhancements are correlated with the energy deposition density (primary ion kinetic energy/area, $\text{keV}/\text{\AA}^2$) at the surface [3]. However, recent studies using Au_n^+ primary ions have suggested that nonlinear yield enhancements are not solely due to an increase in the deposited energy density [4]. To investigate whether the deposited energy density is a major factor in the Bi_n^+ sputtering mechanism, we employed DFT calculations to calculate the structures of Bi_n^+ ($n = 1-6$) (Table 5). From the orientationally-averaged cross-sectional area (Table 5), we calculated the energy density in $\text{keV}/\text{\AA}^2$ deposited into the surface upon impact of a Bi_n^+ assuming that it remains intact. We note that recent MD simulations indicate that Au dimers maintain their identity for at least 50 fs after striking a Si(100) (2×1) surface [30]. The bond energies in a Bi cluster [46,47] are similar to those in a Au cluster [57] and references therein] and thus this is a reasonable

Table 5

The calculated lowest energy structures of bismuth cationic clusters, Bi_n^+ $n = 1-6$, and the orientationally-averaged cross-sectional area of the Bi_n^+ cluster calculated using an atomic radius of 1.60 Å

Number of Bi atoms in the cluster	Structure of the lowest energy Bi_n^+ cluster	Cross-sectional area of the lowest energy Bi_n^+ (\AA^2)
1		8.04
2		14.39
3		20.18
4		25.18
5		30.24
6		35.40

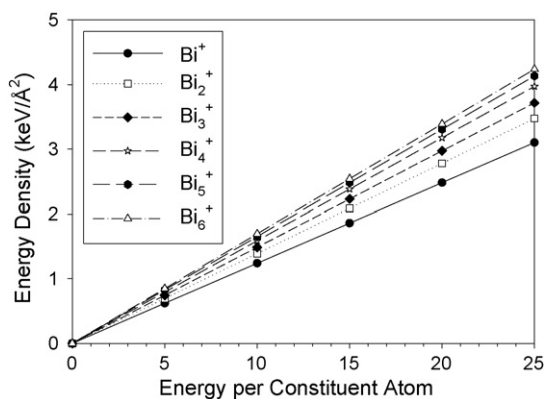


Fig. 6. The energy density, $\text{keV}/\text{\AA}^2$, vs. the energy per particle in the cluster, $1/2 m_{\text{Bi}} v^2$ for the calculated lowest-energy Bi cationic clusters.

assumption. It can be seen in Fig. 6 the energy density deposited into the surface is larger for Bi_n^+ ($n > 2$) than for Bi^+ primary ions, and the slope increases with the number of atoms in the cluster, in agreement with the experimental observations.

However, the changes in the slope are not large enough to account for the nonlinear yield enhancements. The ratios of the slopes (equal to n/A where n = number of atoms in the primary ion and A is the cross-sectional area of the projectile) are 1:1.79:2.51:3.13:3.76:4.40 for $\text{Bi}^+:\text{Bi}_2^+:\text{Bi}_3^+:\text{Bi}_4^+:\text{Bi}_5^+:\text{Bi}_6^+$. Secondly, there is not a large change in slope between Bi^+ , Bi_2^+ and Bi_3^+ primary ions, which is the experimentally observed behavior for the secondary ion yields (Fig. 2). Hence the nonlinear secondary ion yield enhancements observed for Bi_n^+ (and Au_n^+ [4]) primary ions cannot be explained by an increase in the deposited energy density.

Using simple classical mechanics, it can be shown that for a polyatomic projectile at a given kinetic energy the percentage of energy transferred per collision is lower than for the atomic projectile [4,30]. Thus a polyatomic projectile, such as Bi_n^+ or Au_n^+ , will decelerate more slowly than a monoatomic ion. Although the primary ions maintain their identity for some time after collision with the surface [30], as soon as they strike the surface the primary ion should be thought of as a collection of individual atoms with similar velocities. In the near surface region a substrate atom can be struck almost simultaneously by many Bi atoms from a polyatomic projectile, and thus the amount of energy transferred to the substrate is larger than for a Bi^+ primary ion. We note that *although the efficiency of energy transfer is lower, the absolute energy transfer to the substrate atoms is greater for polyatomic Bi ions than for Bi^+ primary ions*. As the Bi_n^+ penetrates deeper into the substrate, the constituent Bi atoms will move further apart and cease to act as a single polyatomic particle. In this regime, the energy transfer rate to the substrate atoms will be similar to that for a monoatomic Bi^+ ion, and so the penetration depth of the polyatomic ion is similar to that for Bi^+ [58]. Thus in the near surface region impacted substrate atoms will have a higher energy than those deeper in the substrate. These higher energy substrate atoms will lead to the ejection of more secondary species and therefore increase the secondary ion yield. Using a larger cluster ion projectile creates more high-velocity substrate atoms and hence there is an

increase in the secondary ion yield as the number of constituent atoms in the primary ion increases. Using geometrical considerations it is unlikely that a single substrate atom will be struck by more than three Bi atoms, and the largest increases in secondary ion yields will be observed in going from Bi^+ to Bi_2^+ to Bi_3^+ , in agreement with experimental observations. This behavior is similar to that observed for Au_n^+ sputtering [4]. At first glance this is surprising since the structures of Bi_n^+ ions are very different to Au_n^+ ions. Bi_n^+ ions are planar for $n = 1-3$ (Table 5) and become three-dimensional at $n > 4$, whereas Au_n^+ ions are planar for $n = 1-7$ [[57] and references therein]. However we note that the orientationally-averaged cross-sectional areas for these ions are very similar and so the likelihood of a substrate atom being struck by multiple projectile atoms is similar.

Using this model, we can also explain the observed substrate effect. For Bi_n^+ primary ions striking an organic film adsorbed on Al, the greater density of Al leads to the earlier break up of the polyatomic Bi_n^+ ion. Consequently, there is a reduction in the energy that is transferred into the near-surface region when compared with Si substrates. Thus, higher secondary ion yields and yield enhancements will be observed on silicon than on aluminum substrates.

5. Conclusions

The use of Bi_n^+ primary ions significantly enhances observed molecular and fragment secondary ion yields when compared to monoatomic Bi primary ion bombardment. We observe that the yield enhancements are largest for molecular and pseudomolecular ions. Further, the secondary ion yield enhancements are, in general, larger on more open surfaces, such as silicon, than on denser ones, such as aluminum.

The mechanism of secondary ion yield enhancement for Bi_n^+ primary ion bombardment is very similar to that for Au_n^+ . The mechanism is complex, and is dependent on many experimental variables including the analyte identity, the underlying substrate structure, the energy density deposited at the surface and the efficiency of energy transfer from the primary ion to the substrate. When a Bi_n^+ primary ion strikes the substrate, its constituent atoms are likely to remain near to each other, and so a substrate atom can be struck simultaneously by multiple Bi atoms. As the Bi_n^+ primary ion penetrates deeper in the substrate, it fragments and a substrate atom is unlikely to be struck by more than one Bi atom. There is therefore more energy deposited into the substrate atoms close to the surface, which leads to the ejection of a larger number of secondary ions. Geometrical considerations show that in the near surface region a substrate atom is unlikely to be struck by more than three constituent atoms of the Bi_n^+ primary ion, and thus the largest differences in secondary ion yield are observed for Bi_2^+ and Bi_3^+ bombardment.

We note that ionization probability for Bi_n^+ primary ion bombardment is lower than for Au_n^+ projectiles. At first glance, this suggests that Au_n^+ primary ions are better for SIMS analyses. However, the use of Bi_n^+ primary ions is advantageous: Bi ion sources produce more cluster ion current and emit larger clusters. This makes it possible to use ions, such as Bi_3^+ , to obtain mass spectrometric images within a reasonable time at very

high lateral resolutions (useful resolution < 500 nm) [21]. Bismuth ion sources also produce doubly-charged species, which can increase both the spatial resolution and improve secondary ion yields [21,56].

Acknowledgements

The authors would like to acknowledge funding from the National Science Foundation (CHE-0518063) and Lev Gelb for help in calculating the cross-sectional areas of the bismuth cluster ions. All calculations were performed using the Washington University Computational Chemistry Facility, supported by NSF grant CHE-0443501.

References

- [1] M.L. Pacholski, N. Winograd, *Chem. Rev.* 99 (1999) 2977.
- [2] J.C. Vickerman, D. Briggs (Eds.), *ToF SIMS: Surface Analysis by Mass Spectrometry*, IM Publications and Surface Spectra Limited, 2001.
- [3] M. Benguerba, A. Brunelle, S. Della-Negra, J. Depauw, H. Joret, Y. Le Beyec, M.G. Blain, E.A. Schweikert, G. Ben Assayag, P. Sudrand, *Nucl. Instrum. Meth. Phys. Res. B* 62 (1991) 8.
- [4] G. Nagy, L.D. Gelb, A.V. Walker, *J. Am. Soc. Mass Spectrom.* 16 (2005) 733.
- [5] K. Boussofiane-Baudin, G. Bolbach, A. Brunelle, S. Della-Negra, P. Håkanson, Y. Le Beyec, *Nucl. Instrum. Methods Phys. Res., Sect. B* 88 (1994) 160.
- [6] K. Boussofiane-Baudin, A. Brunelle, P. Chaurand, S. Della-Negra, J. Depauw, P. Håkanson, Y. Le Beyec, *Nucl. Instrum. Methods Phys. Res., Sect. B* 88 (1994) 61.
- [7] A. Brunelle, S. Della-Negra, J. Depauw, D. Jacquet, Y. Le Beyec, M. Pautrat, K. Baudin, H.H. Andersen, *Phys. Rev. A* 63 (2001) 022902-01-02-10.
- [8] N. Davies, D.E. Weibel, P. Blenkinsopp, N.P. Lockyer, R. Hill, J.C. Vickerman, *Appl. Surf. Sci.* 203–204 (2003) 223.
- [9] P.A. Demirev, J. Eriksson, R.A. Zubarev, R. Papaléo, G. Brinkmalm, P. Håkanson, B.U.R. Sundqvist, *Nucl. Instrum. Methods Phys. Res., Sect. B* 88 (1994) 138.
- [10] F. Kötter, A. Benninghoven, *Appl. Surf. Sci.* 133 (1998) 47.
- [11] G. Gillen, S. Roberson, *Rapid Commun. Mass Spectrom.* 12 (1998) 1303.
- [12] D. Stapel, O. Brox, A. Benninghoven, *Appl. Surf. Sci.* 140 (1999) 156.
- [13] D. Stapel, M. Thiemann, A. Benninghoven, *Appl. Surf. Sci.* 158 (2000) 362.
- [14] A.G. Sostarecz, S. Sun, C. Szakal, A. Wucher, N. Winograd, *Appl. Surf. Sci.* 231–232 (2004) 179.
- [15] S. Sun, C. Szakal, E.J. Smiley, Z. Postawa, A. Wucher, B.J. Garrison, N. Winograd, *Appl. Surf. Sci.* 231–232 (2004) 64.
- [16] N. Winograd, *Anal. Chem.* 77 (2005) 143A.
- [17] M.J. Van Stipdonk, R.D. Harris, E.A. Schweikert, *Rapid Commun. Mass Spectrom.* 10 (1996) 1987.
- [18] S.C.C. Wong, R. Hill, P. Blenkinsopp, N. Lockyer, D.E. Weibel, J.C. Vickerman, *Appl. Surf. Sci.* 203–204 (2003) 219.
- [19] D. Weibel, S. Wong, N. Lockyer, P. Blenkinsopp, R. Hill, J.C. Vickerman, *Anal. Chem.* 75 (2003) 1754.
- [20] R.D. Harris, M.J. Van Stipdonk, E.A. Schweikert, *Int. J. Mass Spectrom. Ion Process.* 174 (1998) 167.
- [21] D. Touboul, F. Kollmer, E. Niehuis, A. Brunelle, O. Laprévote, *J. Am. Soc. Mass Spectrom.* 16 (2005) 1608.
- [22] M.J. van Stipdonk, in: J.C. Vickerman, D. Briggs (Eds.), *ToF-SIMS: Surface Analysis by Mass Spectrometry*, IM Publications and Surface Spectra Limited, 2001, p. 309.
- [23] H.H. Andersen, H.L. Bay, *J. Appl. Phys.* 45 (1974) 953.
- [24] H.H. Andersen, H.L. Bay, *J. Appl. Phys.* 46 (1975) 2416.
- [25] S.S. Johar, D.A. Thompson, *Surf. Sci.* 90 (1979) 319.
- [26] D.A. Thompson, S.S. Johar, *Appl. Phys. Lett.* 34 (1979) 342.
- [27] P. Sigmund, C. Claussen, *J. Appl. Phys.* 52 (1981) 990.
- [28] R. Žaric, B. Pearson, K.D. Krantzman, B.J. Garrison, *Int. J. Mass Spectrom. Ion Process.* 174 (1998) 155.
- [29] R. Žaric, B. Pearson, K.D. Krantzman, B.J. Garrison, in: G. Gillen, R. Lareau, J. Bennett, F. Stevie (Eds.), *Molecular Dynamics Simulations of Organic SIMS with Cluster Projectiles*, SIMS XI, Orlando, USA, 1997, p. 601.
- [30] M. Medvedeva, I. Wojciechowski, B.J. Garrison, *Surf. Sci.* 505 (2002) 349.
- [31] J.A. Townes, A.K. White, K.D. Krantzman, B.J. Garrison, in: J.L. Duggan, I.L. Morgan (Eds.), *Proceedings of the 15th International Conference on the Applications of Accelerators in Research & Industry*, AIP, 1999, p. 401.
- [32] J.A. Townes, A.K. White, E.N. Wiggins, K.D. Krantzman, B.J. Garrison, N. Winograd, *J. Phys. Chem. A* 103 (1999) 4587.
- [33] F. Kollmer, *Appl. Surf. Sci.* 231–232 (2004) 153.
- [34] D. Touboul, F. Halgand, A. Brunelle, R. Kersting, E. Tallarek, B. Hagenhoff, O. Laprévote, *Anal. Chem.* 76 (2004) 1550.
- [35] A.V. Walker, N. Winograd, *Appl. Surf. Sci.* 203–204 (2003) 198.
- [36] J.P. Perdew, J.A. Chevary, S.H. Vosko, K.A. Jackson, M.R. Pederson, D.J. Singh, C. Fiolhais, *Phys. Rev. B* 46 (1992) 6671.
- [37] T.H. Dunning Jr., P.J. Hay, in: H.F. Schaefer III (Ed.), *Methods of Electronic Structure Theory*, Plenum Press, New York, 1975.
- [38] L.F. Pacios, P.A. Christiansen, *J. Chem. Phys.* 82 (1985) 2664.
- [39] M.M. Hurley, L.F. Pacios, P.A. Christiansen, R.B. Ross, W.C. Ermler, *J. Chem. Phys.* 84 (1986) 6840.
- [40] L.A. LaJohn, P.A. Christiansen, R.B. Ross, T. Atashroo, W.C. Ermler, *J. Chem. Phys.* 87 (1987) 2812.
- [41] R.B. Ross, J.M. Powers, T. Atashroo, W.C. Ermler, L.A. LaJohn, P.A. Christiansen, *J. Chem. Phys.* 93 (1990) 6654.
- [42] W.C. Ermler, R.B. Ross, P.A. Christiansen, *Int. J. Quantum Chem.* 40 (1991) 829.
- [43] T.P. Straatsma, E. Aprà, T.L. Windus, M. Dupuis, E.J. Bylaska, W. de Jong, S. Hirata, D.M.A. Smith, M. Hackler, L. Pollack, R. Harrison, J. Nieplocha, V. Tipparaju, M. Krishnan, E. Brown, G. Cisneros, G. Fann, H. Fruchtl, J. Garza, K. Hirao, R. Kendall, J. Nichols, K. Tsemekhman, M. Valiev, K. Wolinski, J. Anchell, D. Bernholdt, P. Borowski, T. Clark, D. Clerc, H. Daschel, M. Deegan, K. Dyall, D. Elwood, E. Glendening, M. Gutowski, A. Hess, J. Jaffe, B. Johnson, J. Ju, R. Kobayashi, R. Kutteh, Z. Lin, R. Littlefield, X. Long, B. Meng, T. Nakajima, S. Niu, M. Rosing, G. Sandrone, M. Stave, H. Taylor, G. Thomas, J. van Lenthe, A. Wong, Z. Zhang, N.W. Chem, A Computational Chemistry Package for Parallel Computers, Pacific Northwest National Laboratory, Richland, Washington 99352-0999, USA, 2003.
- [44] D.R. Lide (Ed.), *CRC Handbook of Chemistry and Physics*, CRC Press, 2003.
- [45] R.E. Walstedt, R.F. Bell, *Phys. Rev. A* 33 (1986) 2830.
- [46] F.J. Kohl, K.D. Carlson, *J. Am. Chem. Soc.* 90 (1968) 4814.
- [47] P.Y. Cheng, K.F. Willey, J.E. Salicido, M.A. Duncan, *Int. J. Mass Spectrom. Ion Process.* 102 (1990) 67.
- [48] P.J. Hay, W.R. Wadt, *J. Chem. Phys.* 82 (1985) 270.
- [49] W.R. Wadt, P.J. Hay, *J. Chem. Phys.* 82 (1985) 284.
- [50] P.J. Hay, W.R. Wadt, *J. Chem. Phys.* 82 (1985) 299.
- [51] A.N. Kuznetsov, L. Kloos, M. Lindsjö, J. Rosdahl, H. Stoll, *Chem. Eur. J.* 7 (2001) 2821.
- [52] K. Wade, *Chem. Commun.*, (1971) 792.
- [53] K. Wade, *Chem. Br.* 11 (1975) 177.
- [54] J.C. Slater, *J. Chem. Phys.* 41 (1964) 3199.
- [55] J.C. Vickerman, A.R. Brown, N.M. Reed, *Secondary Ion Mass Spectrometry: Principles and Applications*, Clarendon Press, Oxford, 1989.
- [56] G. Nagy, A.V. Walker, in preparation.
- [57] A.V. Walker, *J. Chem. Phys.* 122 (2005) art. no. 094310.
- [58] H.H. Andersen, A. Johansen, M. Olsen, V. Touboltsev, *Nucl. Instrum. Meth. Phys. Res. B* 212 (2003) 56.